Desalination and Water Treatment
www.deswater.com
doi: 10.5004/dwt.2020.25171

182 (2020) 253–259
April

Visible light-driven photocatalytic properties of BiOI-based photocatalyst prepared by different solvents

Zhao Li[a], Jiao Huang[a], Junbo Zhong[a,b,*], Jianzhang Li[a,*]

[a]*Key Laboratory of Green Catalysis of Higher Education Institutes of Sichuan, College of Chemistry and Environment Engineering, Sichuan University of Science and Engineering, Zigong, 643000, China, emails: junbozhong@163.com (J. Zhong), lschmanuscript@163.com (J. Li), 1211801868@qq.com (Z. Li), 1054617557@qq.com (J. Huang)*
[b]*College of Chemical Engineering, Sichuan University of Science and Engineering, Zigong, 643000, China*

Received 13 June 2019; Accepted 13 November 2019

ABSTRACT

In this study, BiOI photocatalysts were prepared by a solvothermal method using different solvents (glacial acetic acid, ethylene glycol, and glycerol), and Bi_2O_3/BiOI composite photocatalysts were obtained after high-temperature treatment using ethylene glycol and glycerol as a solvent. The prepared photocatalysts were characterized by X-ray diffraction, scanning electron microscopy, high-resolution transmission electron microscopy, diffuse reflectance spectroscopy, and Brunauer–Emmett–Teller. The photocatalytic activities of the samples were evaluated by the degradation of rhodamine B (RhB) under visible light irradiation. The results reveal that BiOI-based photocatalyst prepared using glycerol as a solvent displays the highest photocatalytic activity.

Keywords: BiOI; Photocatalyst; Solvents; RhB; Separation rate of photoinduced carriers

1. Introduction

Extensive application of organic dyes has caused serious water pollution. These organic dyes are highly toxic, carcinogenic and teratogenic, therefore the organic dyes are harmful to human health. Moreover, organic dyes have high chemical stability and complex composition, and it is very difficult to treat these organic dyes [1–4]. As a reliable technology-driven by sunlight, photocatalysis has the advantages of strong oxidation ability, high degree of degradation, green and safe. Photocatalytic technology can degrade organic dyes into CO_2 and H_2O and has promising application prospect in organic dye wastewater treatment [5–7]. Among the photocatalyst developed, BiOI is a prospective photocatalyst with a prominently visible light response. BiOI has a narrow bandgap (1.8 eV), strong absorption in the visible light region, and a layered structure formed by I atom and $[Bi_2O_2]^{2+}$. The layered structure is beneficial to the separation of photogenerated electron-hole pairs [8–10]. However, the photoinduced electron-hole pair of BiOI has a fast recombination rate and a slow charge transfer rate, which significantly hinders the practical application of BiOI [11–14]. Lu et al. [15] found that the solvent viscosity has an evident effect on the growth of the product, and the microsphere-like BiOI can be prepared using a high viscosity solvent. Generally, the sequence of photocatalytic activity of BiOI is hollow BiOI > spherical BiOI > flake BiOI, hollow and spherical BiOI photocatalysts have high specific surface area and special mesoporous structure [16,17]. Xiao et al prepared BiOI/Bi_4O_5I composites, remarkably improving the separation rate of photogenerated electron-hole pairs by combustion method [18].

Inspired by the above results, in this work, the morphology of BiOI was controlled by different solvents, and BiOI/Bi_2O_3 composite photocatalysts were fabricated by high-temperature calcination, and high separation rate of photogenerated

* Corresponding authors.

electron-hole pair was achieved. Photocatalytic degradation of rhodamine B (RhB) over BiOI-based photocatalysts under visible light irradiation was investigated. The results show that the BiOI/Bi_2O_3 composite photocatalyst prepared using glycerol as a solvent has the highest photocatalytic activity.

2. Experimental

2.1. Preparation of the samples

5 g Bi $(NO_3)_3{\cdot}5H_2O$ was dissolved in 40 ml of glacial acetic acid (HAc), ethylene glycol (EG) and glycerol (GL), respectively, and then was sonicated for 30 min. 20 ml KI aqueous solution (0.5155 mmol/L) was added into the Bi^{3+}-HAc, Bi^{3+}-EG and Bi^{3+}-GL solution under vigorous stirring, respectively, then was continually stirred for 30 min. The mixture was transferred to a 100 mL Teflon-lined stainless autoclave and maintained at 453 K for 24 h. After the autoclave was naturally cooled to room temperature, the solid formed was collected by filtration, rinsed with deionized water and absolute ethanol several times. Finally, the samples were dispersed into absolute ethanol and then dried in an oven at 333 K for 6 h. To remove the residual organics, the samples were baked at 673 K for 2 h.

2.2. Characterization of the samples

Powder X-ray diffraction (XRD) patterns of the sample were analyzed on a DX-2600 X-ray diffractometer using Cu-Ka radiation (0.15406 nm) with a scanning range of 10°–70° and a scanning speed of 0.03° s^{-1}, the analysis was operated at 35 kV and 25 mA. UV-Vis diffuse reflectance spectroscopy (DRS) of the samples was recorded on a UH-4150 UV-Vis spectrophotometer using barium sulfate as a reference. Surface photovoltage spectroscopy (SPS) of the samples was measured on a surface photovoltage spectrometer (MODEL SR540) in the range of 300–600 nm. Scanning electron microscopy (SEM) images of the samples were observed on a VEGA 3 SBU SEM with an accelerating voltage of 15 kV. The high-resolution transmission electron microscopy (HRTEM) information of the samples was obtained on a JEOL-2100 microscope at an acceleration voltage of 200 kV. The specific surface area of the sample was measured on an SSA-4200 automatic surface analyzer using the Brunauer–Emmett–Teller (BET) method. The electron spin-resonance (ESR) experiments were performed on a Bruker E 500 using 5,5-dimethyl-1-pyrroline-N-oxide (DMPO) as capture.

2.3. Photocatalytic tests

In this demonstration, RhB was used as a model dye. Photocatalytic activities of the samples were evaluated by the degradation of RhB under visible light irradiation. The photocatalytic experiments were performed in a photochemical reactor (CEL-LB70-3, Beijing Zhongjiao Jinyuan Technology Co., Ltd., China). The visible light was provided by a 500 W Xe lamp with a 420 nm cutoff filter. 40 mg of the sample and 40 mL RhB aqueous solution (10 mg/L) were added into a 50 mL quartz reactor with a recycling water glass jacket to keep the reaction temperature at 298 K, and then was stirred in dark for 30 min to establish adsorption-desorption equilibrium, then the suspension system was irradiated by visible light (the distance between lamp and quartz reactor is 15 cm). At regular intervals, 5 ml of the suspension was sampled for analysis. The residual concentration of RhB was measured at 554 nm on a UV-visible spectrophotometer.

3. Results and discussion

3.1. Characterization of the samples

Fig. 1 shows the XRD patterns of all the samples and Bi_2O_3. The typical characteristic peaks of BiOI-HAc at 19.6°, 29.65°, 31.66°, 39.36°, 45.38°, and 55.2° correspond to the (002), (102), (110), (004), (200) and (212) planes of BiOI, respectively, and these peaks can be indexed to the tetragonal BiOI (JCPDS File No.10-0445) [19,20]. The (002) and (004) planes were not observed in BiOI-EG and BiOI-Gl. Compared with the (102) plane of BiOI-HA, the full width at half maximum (FWHM) of BiOI-EG and BiOI-GL gradually increases, indicating that the crystal size becomes small. The above results show that the solvent viscosity significantly affects the crystal size and the growth direction of the crystal plane. Furthermore, for BiOI-EG and BiOI-GL, no peaks of Bi_2O_3 were detected due to the low content of Bi_2O_3.

SEM images of BiOI-based photocatalysts prepared with the assistance of different solvents are shown in Fig. 2. BiOI-HAc is a sheet-like shape, which can be attributed to the layered structure of BiOI. For BiOI-EG, the morphology is irregular sheet and sheet assembled-sphere, while for BiOI-GL, the shape is irregular lump and sheet assembled-sphere in part. The results display that BiOI-based photocatalysts prepared using different solvents exhibit different morphology. When glacial acetic acid was used as a solvent, since glacial acetic acid has low viscosity, the ions can easily diffuse, thus BiOI tends to grow into a sheet. However, when ethylene glycol and glycerol were employed as solvent, in light of relatively high viscosity, the ions cannot easily diffuse; consequently, sheet-like BiOI assembles into an irregular sphere by Ostwald ripening [15].

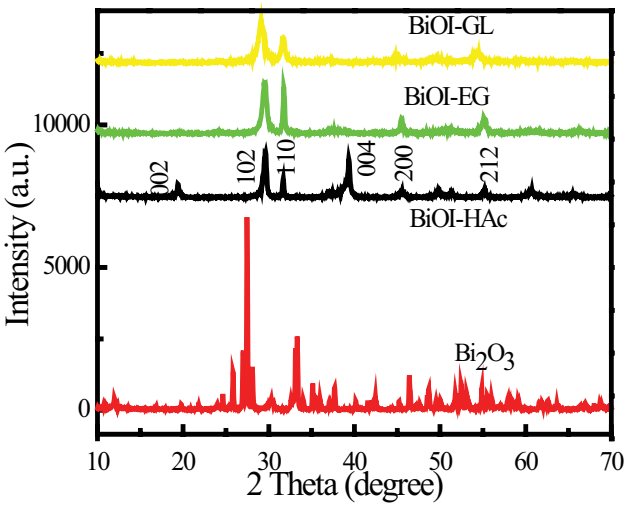

Fig. 1. XRD profiles of the samples.

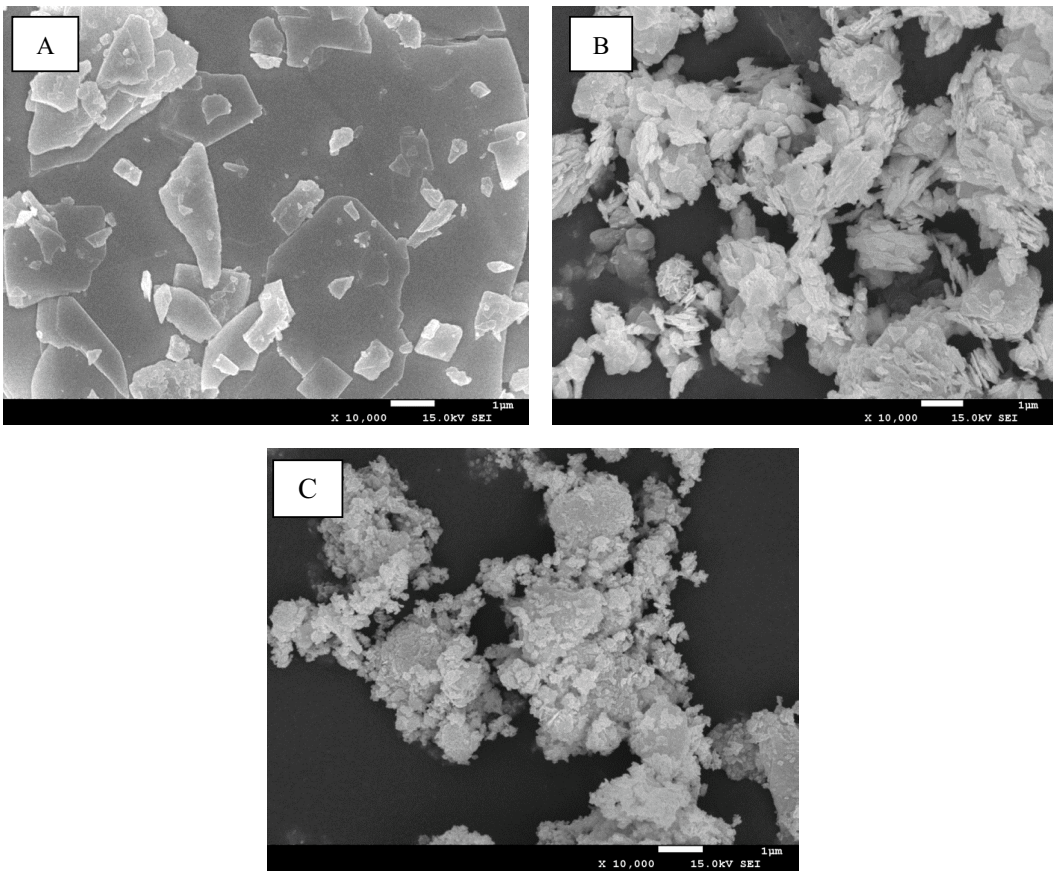

Fig. 2. SEM of the samples (a) BiOI-HAc, (b) BiOI-EG, and (c) BiOI-GL.

HRTEM images of BiOI-based photocatalysts prepared by the different solvents are demonstrated in Fig. 3. As shown in Fig. 3, the lattice spacing of 0.294, 0.363, and 0.240 nm was observed, which can be assigned to the (102), (101) and (112) crystal planes of BiOI (JCPDS No. 10-0445) [4,21]. The lattice spacing of 0.345 nm and 0.312 nm corresponds to the (002) and (012) planes of Bi_2O_3 (JCPDS No. 41-1449), respectively [22], indicating that the sample prepared using ethylene glycol and glycerol as solvent contain Bi_2O_3. Bi_2O_3 is formed by the reaction of metallic bismuth with oxygen at high temperature, metallic bismuth originates from the reduction of Bi^{3+} by ethylene glycol and glycerol during the process of solvothermal treatment [23].

The specific surface area of the sample preparation was tested by the BET method. As shown in Table 1, the solvent affects the specific surface area of the BiOI-based catalyst, suggesting that the specific surface area of the photocatalysts can be effectively altered by the solvent. In this case, BiOI prepared using glycerol as a solvent has the highest specific surface area; high specific surface area can provide more active sites and adsorb more pollutants, which is conducive to the photocatalytic performance.

Optical properties of BiOI-based photocatalysts prepared by different solvents were studied by UV-Vis absorption spectroscopy (DRS). As shown in Fig. 4a. Compared with BiOI-HAc, BiOI-EG and BiOI-GL photocatalysts appear blue-shift, which demonstrates that these two BiOI-based samples have wider bandgap than BiOI-HAc due to the presence of Bi_2O_3 in the samples [24]. The bandgap energy can be calculated by the following formula [25–27]: $\alpha h\nu = A(h\nu\text{-}Eg)^{n/2}$, where α, h, ν, A and Eg are the absorption coefficient, the Planck constant, the optical frequency, the proportionality constant and the bandgap, respectively. The value of n in this formula is determined by the semiconductor type of the sample. The bandgap of these samples can be obtained by plotting a curve of $(\alpha h\nu)^{1/2}$ vs. $h\nu$. As shown in Fig. 4b, the band gaps of BiOI-HAc, BiOI-EG, BiOI-GL are 1.50, 1.70, and 1.70 eV, respectively. The band edge potentials of conduction band (CB) and valence band (VB) of the catalysts were calculated by a simple formula. The formula is $E_{VB} = X - E^e + 0.5Eg$, $E_{CB} = E_{VB} - Eg$, where E_{VB} and E_{CB} represent VB edge potential and CB edge potential. X is the electronegativity of the semiconductor (the geometric mean of the electronegativity of the constituent atom), E^e is the energy of the free-electron on the hydrogen order of magnitude (~4.5 eV), Eg is the bandgap [28,29]. The X values for BiOI and Bi_2O_3 are 5.94 and 6.23 eV, respectively [30]. The E_{VB} and E_{CB} of BiOI are calculated to be 2.29 and 0.59 eV, respectively. The E_{VB} and E_{CB} of Bi_2O_3 are 2.75 and 0.71 eV, respectively.

The surface photovoltaic characteristics of the samples were investigated by SPS. As shown in Fig. 5, BiOI-GL has the strongest SPS response from 300–500 nm. However, from 500–600 nm, BiOI-HAc holds the strongest SPS response. According to the principle of SPS, strong SPS response originates from a high separation rate of photogenerated carriers. Therefore, from 300–500 nm, the separation rate of

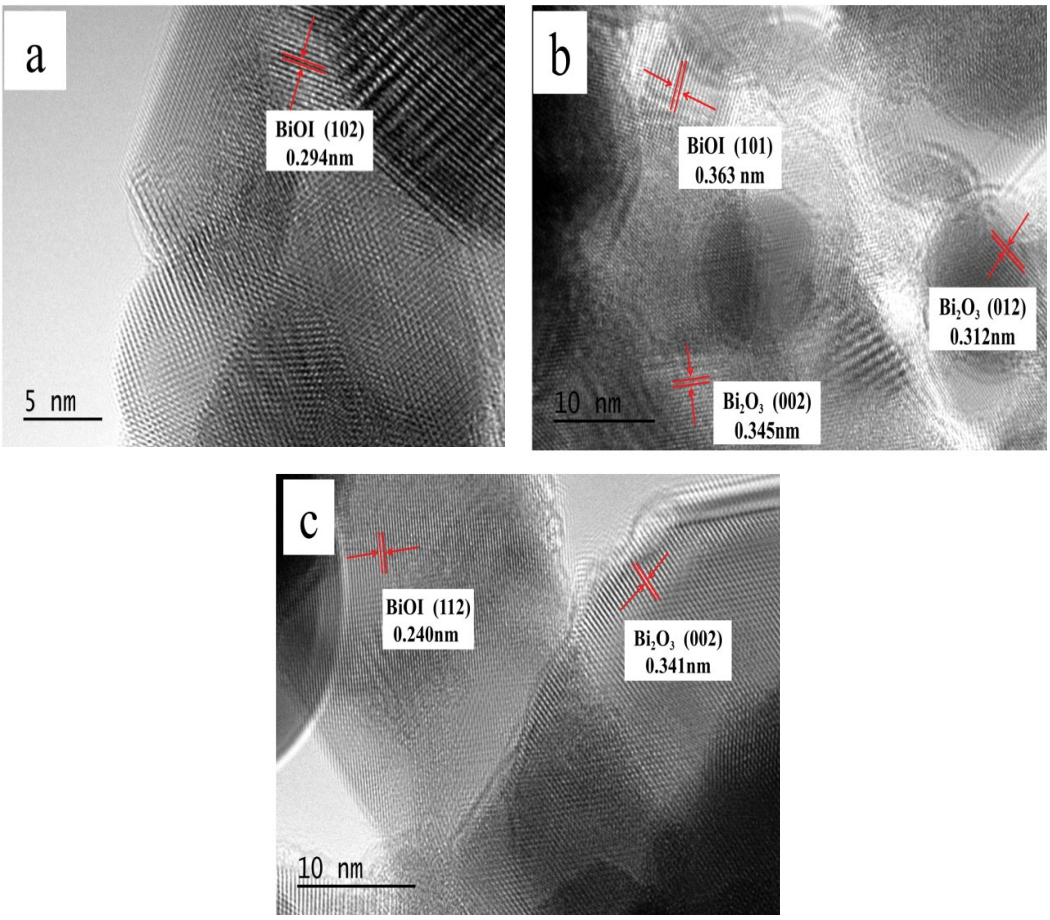

Fig. 3. HRTEM of the samples (a) BiOI-HAc, (b) BiOI-EG, and (c) BiOI-GL.

Table 1
Texture properties of the samples

Samples	S_{BET} (m^2/g)	Pore volume (cc/g)	Pore diameter (nm)
BiOI-HAc	5.0	0.0021	1.68
BiOI-EG	11.4	0.0059	2.08
BiOI-GL	18.7	0.0095	2.04

photogenerated carriers of BiOI-GL is the highest. High photocatalytic performance can be benefited from a high separation rate of photogenerated carriers [28,31,32], which accords well with the results of the photocatalytic test.

To reveal the active free radicals produced in the photocatalytic system under visible light irradiation, trapping experiments were performed. The scavengers used in this experiment are benzoquinone (BQ for $^{\bullet}O_2^-$), isopropanol (IPA, for $^{\bullet}OH$) and ammonium oxalate (AO, for h^+) [28–31]. As shown in Fig. 6a, the effect of IPA on the degradation efficiency of RhB is negligible, which indicates that $^{\bullet}OH$ is not the main active free radicals during the photocatalytic degradation of RhB or no $^{\bullet}OH$ was formed. However, after the addition of BQ and AO, the degradation efficiency of RhB is 75% and 70%, respectively. The photocatalytic degradation efficiency of RhB is significantly inhibited, indicating that $^{\bullet}O_2^-$ and h^+ are major active free radicals. To further ascertain the presence of active free radicals, the ESR experiment was performed. DMPO was added to the BiOI-GL photocatalytic system. Seen Fig. 6b, strong signals of DMPO-$^{\bullet}O_2^-$ were detected, further indicating that $^{\bullet}O_2^-$ is the main active free radicals, which accords well with the results of trapping experiments. However, no signals of DMPO-$^{\bullet}OH$ were detected, firmly proving that no $^{\bullet}OH$ radicals were produced in the photocatalytic process [31,32].

To further determine the presence of $^{\bullet}O_2^-$ in the catalytic system and to elaborate the separation rate of photogenerated electron-hole pairs, nitrotetrazolium blue (NBT) experiments were carried out. NBT can react with the $^{\bullet}O_2^-$, resulting in low NBT concentration. NBT was added to the different photocatalytic systems, the absorption spectrum of NBT was measured under visible light irradiation for 1 h. The spectral change of NBT is shown in Fig. 6c. The low absorption peak of NBT in the photocatalytic system corresponds to a high separation rate of photogenerated electron-hole pairs. The absorption peaks of NBT over all the samples remarkably decreases, indicating that $^{\bullet}O_2^-$ exist in the photocatalytic reaction system. The absorption peak of NBT over BiOI-GL is the lowest, indicating that the photo-generated electron-hole pairs of BiOI-GL has the highest separation rate, which fits well with the results of SPS [29,30].

The separation and transfer of photogenerated carriers play a key role in influencing the catalytic performance

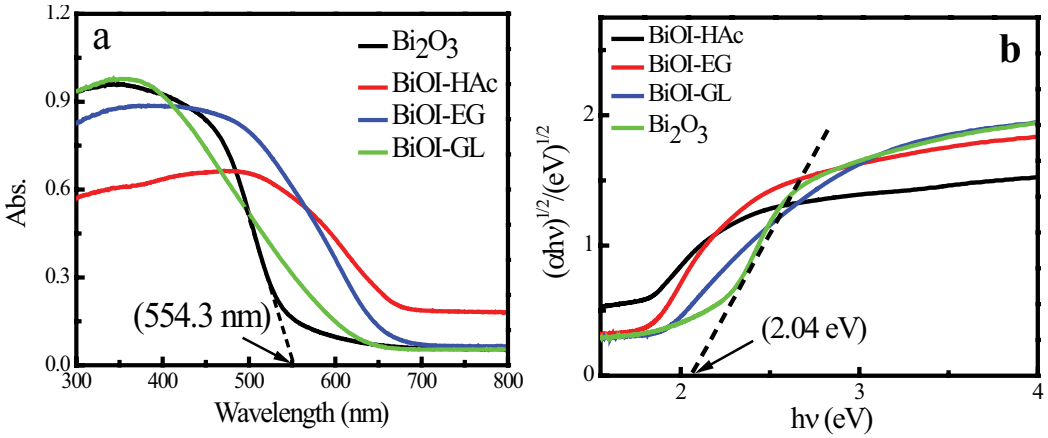

Fig. 4. (a) UV-Vis DRS of BiOI-HAc, BiOI-EG, BiOI-GL and Bi_2O_3 and (b) plots of $(\alpha h\nu)^{1/2}$ vs. photon energy ($h\nu$) of the corresponding samples.

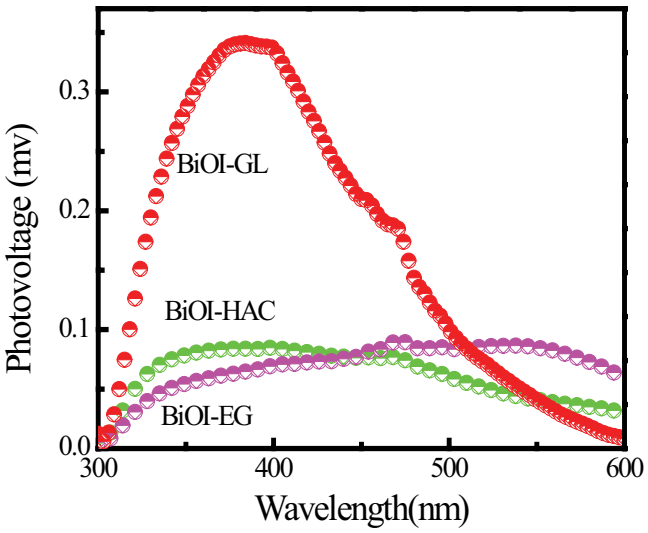

Fig. 5. SPS spectra of the photocatalysts.

of photocatalysts [31]. Therefore, it is necessary to understand the behavior of photogenerated carriers in the Bi_2O_3-BiOI composite. Fig. 7 briefly discusses the separation and transfer of photogenerated carriers of Bi_2O_3-BiOI composite. Under visible light irradiation, BiOI and Bi_2O_3 can be excited. The electrons from VB of BiOI can be excited to a higher edge potential (–0.56 eV) [32]. The potential for $O_2/{}^{\bullet}O_2^-$ is –0.33 eV, thus the electrons from CB of BiOI can react with O_2 adsorbed on the catalyst surface to yield ${}^{\bullet}O_2^-$. The photogenerated electrons from CB of Bi_2O_3 combine with the holes from VB of BiOI [30–34]. The VB potential of Bi_2O_3 (2.75 eV) is lower than that of $H_2O/{}^{\bullet}OH$ (2.77 eV), so the hole of Bi_2O_3 cannot oxidize water to produce hydroxyl radicals, thus no DMPO-${}^{\bullet}OH$ signals were detected in ESR experiment. According to Fig. 7, the separation and transfer of photogenerated carriers follow a Z-scheme. Following Z-scheme, the photo-generated electrons and holes can be well separated, effectively inhibiting the recombination of photogenerated electron-hole pairs, thus improving the catalytic performance of the photocatalysts [32–34].

3.2. Photocatalytic performance

The photocatalytic activity of the prepared samples was evaluated by the degradation of RhB under visible light irradiation. Before the photocatalytic reaction, the suspension was stirred in the dark for 30 min to achieve adsorption–desorption equilibrium. BiOI-EG and BiOI-GL have a high specific surface area and can absorb more pollutants on the surface of the samples, which is beneficial to the photocatalytic reaction. Fig. 8 shows the photocatalytic degradation of RhB over four different photocatalysts under visible light irradiation. It can be seen that BiOI-GL has the highest photocatalytic performance, and the degradation efficiency of RhB over BiOI-GL is 99.3% after 25 min visible light illumination, and the degradation efficiency of RhB over BiOI-EG, BiOI-HAc, and Bi_2O_3 is 97.1%, 28.5% and 38.2% after 25 min, respectively. The results are consistent with the results of SPS, further indicating that the separation efficiency of photogenerated electron-hole is one of the main factors affecting the photocatalytic performance of photocatalyst. The relationship between concentration of RhB and irradiation time can be expressed as pseudo-first-order kinetics: $\ln(C_0/C_t) = kt$ [12], where k is a pseudo-first-order rate constant, C_0 and C_t is the RhB concentration at 0 and t min, respectively. The apparent rate constant of RhB on the sample was shown in Fig. 8b. The apparent rate constant of RhB over BiOI-HAc, BiOI-EG, BiOI-GL, and Bi_2O_3 is 0.01, 0.115, 0.161, and 0.015 min^{-1}, respectively. The photocatalytic performance of BiOI-GL is 16 times that of BiOI-HAc. The photocatalytic performance of BiOI/Bi_2O_3 composite photocatalysts can be significantly improved by using glycerol as a solvent.

4. Conclusions

In summary, BiOI-based photocatalysts were successfully prepared by a solvothermal method using different solvents. The effects of different solvents on the preparation and photocatalytic performance of BiOI were analyzed. The experimental results show that the preparation of BiOI using glycerol as a solvent can control the morphology of BiOI, which can significantly improve the separation efficiency of photoinduced carriers. According to the photocatalytic performance test under visible light irradiation, BiOI-GL

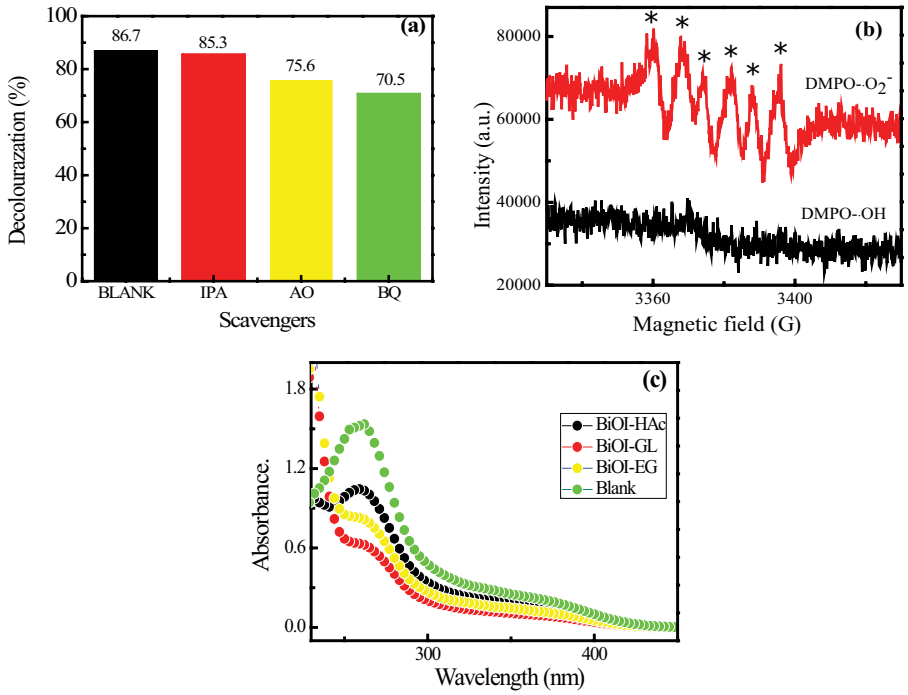

Fig. 6. (a) Photocatalytic decolorization efficiency of RhB on the BiOI-GL sample in the presence of different scavengers (irradiation time = 1 h), (b) DMPO-•OH and DMPO-•O_2^- signals of the BiOI-GL sample under Xe lamp irradiation for 2 min, and (c) NBT spectra in different photocatalytic systems.

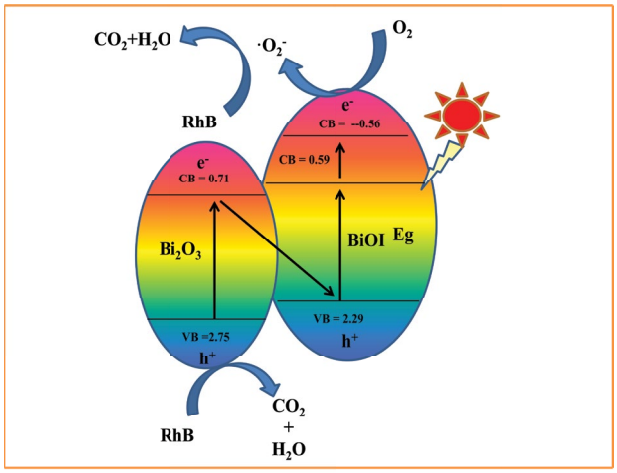

Fig. 7. Separation and transfer of photogenerated carriers.

has the highest photocatalytic activity, which accords well with the SPS results. The heterojunctions between Bi_2O_3 and BiOI accelerates the separation of photogenerated carriers, forming a high level of active free radicals and thereby improving the photocatalytic performance. This study can be used to prepare other photocatalysts, providing a feasible method and good solvent selection for the preparation of high-efficiency photocatalysts.

Acknowledgments

This project was supported financially by the Opening Project of Jiangsu Key Laboratory for Environment Functional

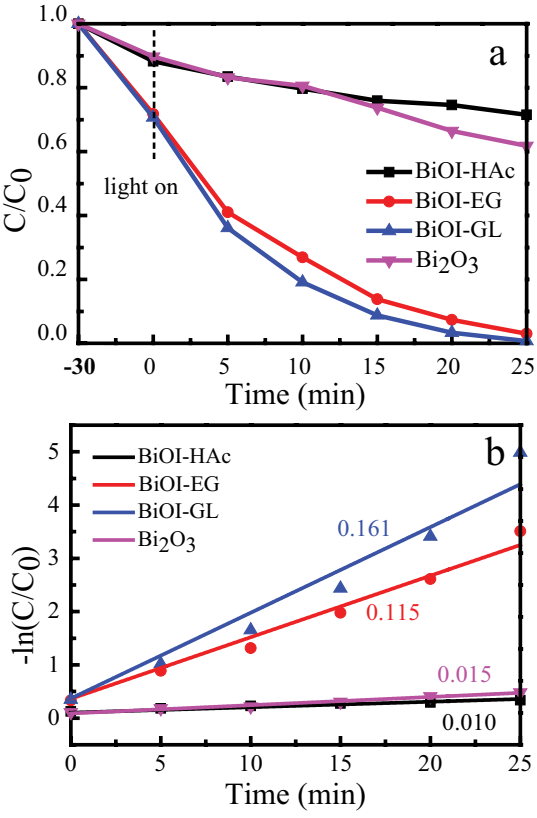

Fig. 8. Adsorption and visible-light-degradation curve of RhB on photocatalyst (a) and its corresponding pseudo-first-order kinetic curve (b).

Materials (SJHG1805) and Opening Project of Key Laboratory of Green Catalysis of Sichuan Institutes of High Education (No. LYJ1603) and Graduate student Innovation Fund of Sichuan University of Science and Engineering (y2019027).

References

[1] M.G. Wang, J. Han, Y.M. Hu, R. Guo, Y.D. Yin, Carbon-incorporated NiO/TiO_2 mesoporous shells with p-n heterojunctions for efficient visible light photo-catalysis, ACS Appl. Mater. Interfaces, 8 (2016) 29511–29521.

[2] L. Wang, Y.Y. Wan, Y.J. Ding, S.K. Wu, Y. Zhang, X.L. Zhang, G.G. Zhang, Y.J. Xiong, X.J. Wu, J.L. Yang, X.G. Xu, Conjugated microporous polymer nanosheets for overall water splitting using visible light, Adv. Mater., 29 (2017) 1–8.

[3] J. Tian, Z.W. Chen, X.Y. Deng, Q. Sun, Z.Y. Sun, W.B. Li, Improving visible light driving degradation of norfloxacin over core-shell hierarchical BiOCl microspherical photocatalyst by synergistic effect of oxygen vacancy and nanostructure, Appl. Surf. Sci., 453 (2018) 373–382.

[4] J.Y. Liu, H.P. Li, N. Du, S. Song, W.G. Hou, Synthesis characterization and visible-light photocatalytic activity of BiOI hierarchical flower-like microspheres, RSC Adv., 4 (2014) 31393–31399.

[5] R. Michal, E. Dworniczek, M. Caplovicova, O. Monfort, P. Lianos, L. Caplovic, G. Plesch, Photocatalytic properties and selective antimicrobial activity of TiO_2(Eu)/CuO nanocomposite, Appl. Surf. Sci., 371 (2016) 538–546.

[6] S.J. Darzi, A.R. Mahjoub, A. Bayat, Synthesis and characterization of visible light active S-doped TiO_2 nanophotocatalyst, Int. J. Nano Dimens., 45 (2016) 1254–1261.

[7] X.F. Qu, Y.D. Yi, F.Y. Qiao, M.H. Liu, X.R. Wang, R. Yang, H.H. Meng, L. Shi, F.L. Du, TiO_2/BiOI/CQDs: enhanced photocatalytic properties under visible-light irradiation, Ceram. Int., 44 (2018) 1348–1355.

[8] S.M. Wang, Y. Guan, L.P. Wang, W. Zhao, H. He, J. Xiao, S.G. Yang, C. Sun, Fabrication of a novel bifunctional material of BiOI/Ag_3VO_4 with high adsorption-photocatalysis for efficient treatment of dye wastewater, Appl. Catal., B, 168 (2015) 448–457.

[9] J.B. Sun, J.R. Song, M.A. Gondal, S. Shi, Z.X. Lu, Q.Y. Xu, X.F. Chang, D.H. Xiang, K. Shen, Preparation of g-C_3N_4/BiOX (X = Cl, Br, I) composites and their photocatalytic activity under visible light irradiation, Res. Chem. Intermed., 41 (2015) 6941–6955.

[10] Z.D. Wei, R.S. Li, R. Wang, Enhanced visible light photocatalytic activity of BiOBr by in situ reactable ionic liquid modification for pollutant degradation, RSC Adv., 8 (2018) 7956–7962.

[11] P. Intaphong, A. Phuruangrat, S. Thongtem, T. Thongtem, Sonochemical synthesis and characterization of BiOI nanoplates for using as visible-light-driven photocatalyst, Mater. Lett., 213 (2018) 88–91.

[12] H.B. Song, R.Y. Wu, J.F. Yang, J.C. Dong, G.J. Ji, Fabrication of CeO_2 nanoparticles decorated three-dimensional flower-like BiOI composites to build p-n heterojunction with highly enhanced visible-light photocatalytic performance, J. Colloid Interface Sci., 512 (2018) 325–334.

[13] H.F. Cheng, B.B. Huang, Y. Dai, Engineering BiOX (X = Cl, Br, I) nanostructures for highly efficient photocatalytic applications, Nanoscale, 6 (2014) 2009–2026.

[14] N. Huang, J.X. Shu, Z.H. Wang, M. Chen, C.G. Ren, W. Zhang, One-step pyrolytic synthesis of ZnO nanorods with enhanced photocatalytic activity and high photostability under visible light and UV light irradiation, J. Alloys Compd., 648 (2015) 919–929.

[15] B. Lu, S. Zeng, C.Y. Li, Y.Z. Wang, X.H. Pan, L. Zhang, H.Y. Mao, Y.H. Lu, Z.Z. Ye, Nanoscale p-n heterojunctions of BiOI/nitrogen-doped reduced graphene oxide as a high performance photocatalyst, Carbon, 132 (2018) 191–198.

[16] J. Hu, S.X. Weng, Z.Y. Zheng, Z.X. Pei, M.L. Huang, P. Liu, Solvents mediated-synthesis of BiOI photocatalysts with tunable morphologies and their visible-light driven photocatalytic performances in removing of arsenic from water, J. Hazard. Mater., 264 (2014) 293–302.

[17] J. Di, J.X. Xia, Y.P. Ge, X. Li, X. Hui, M.Q. He, Q. Zhang, H.M. Li, Reactable ionic liquid-assisted rapid synthesis of BiOI hollow microspheres at room temperature with enhanced photocatalytic activity, J. Mater. Chem. A, 2 (2014) 15864–15874.

[18] X.J. Xiao, Y. Lin, B.L. Pan, W.J. Fan, Y.C. Huang, Photocatalytic degradation of methyl orange by BiOI/$Bi_4O_5I_2$, microspheres under visible light irradiation, Inorg. Chem. Commun., 93 (2018) 65–68.

[19] J. Lu, J. Wu, W.X. Xu, H.Q. Cheng, X.M. Qi, Q.W. Li, Y.N. Zhang, Y. Guan, Y. Ling, Z. Zhang, Room temperature synthesis of tetragonal BiOI photocatalyst with surface heterojunction between (0 0 1) facets and (1 1 0) facets, Mater. Lett., 219 (2018) 260–264.

[20] J.F. Niu, P.X. Dai, Q. Zhang, B.H. Yao, X.J. Yu, Microwave-assisted solvothermal synthesis of novel hierarchical BiOI/rGO composites for efficient photocatalytic degardation of organic pollutants, Appl. Surf. Sci., 430 (2018) 165–175.

[21] K.H. Reddy, S. Martha, K. Parida, Fabrication of novel p-BiOI/n-$ZnTiO_3$ heterojunction for degradation of rhodamine 6G under visible light irradiation, Inorg. Chem., 52 (2013) 6390–6401.

[22] T. Chen, Q. Hao, W.J. Yang, C.L. Xie, D.M. Chen, C. Ma, W.Q. Yao, Y.F. Zhu, A honeycomb multilevel structure Bi_2O_3 with highly efficient catalytic activity driven by bias voltage and oxygen defect, Appl. Catal., B, 237 (2018) 442–448.

[23] G.Q. Zhu, M. Hojamberdiev, S.H. Zhang, S.T.U. Din, W. Yang, Enhancing visible-light-induced photocatalytic activity of BiOI microspheres for NO removal by synchronous coupling with Bi metal and graphene, Appl. Surf. Sci., 468 (2019) 968–978.

[24] Z.Y. Jiang, X.Z. Liang, Y.Y. Liu, T. Jing, Z.Y. Wang, X.Y. Zhang, X.Y. Qin, Y. Dai, B.B. Hang, Enhancing visible light photocatalytic degradation performance and bactericidal activity of BiOI via ultrathin-layer structure, Appl. Catal., B, 211 (2017) 252–257.

[25] C. Liang, C.G. Niu, H. Guo, D.W. Huang, X.J. Wen, S.F. Yang, G.M. Zeng, Combination of efficient charge-separation process with the assistance of novel dual Z-scheme system: self-assembly photocatalyst of Ag@AgI/BiOI modified oxygen-doped carbon nitride nanosheet with enhanced photocatalytic performance, Catal. Sci. Technol., 8 (2018) 1161–1175.

[26] C.X. Zhou, H.W. Yang, G. Wang, J.W. Chen, R.L. Wang, C.P. Jiang, BiOI-promoted nano-on-micro BiOI-MoS_2/CdS system for high-performance on photocatalytic H_2 evolution under visible light irradiation, Int. J. Hydrogen Energy, 42 (2017) 2837–28348.

[27] H.W. Huang, X.W. Li, X. Han, N. Tian, Y.H. Zhang, T.R. Zhang, Moderate band-gap-broadening induced high separation of electron-hole pairs in Br substituted BiOI: a combined experimental and theoretical investigation, Phys. Chem. Chem. Phys., 17 (2015) 3673–3681.

[28] J. Huang, H.H. Liu, J.B. Zhong, Q. Yang, J.F. Chen, J.Z. Li, D.M. Ma, R. Duan, Enhanced sunlight-driven photocatalytic performance of Bi-doped $CdMoO_4$ benefited from efficient separation of photogenerated charge pairs, Solid State Sci., 80 (2018) 147–154.

[29] H.B. Li, Z.J. Yang, J.N. Zhang, Y.C. Huang, H.B. Ji, Y.X. Tong, Indium doped BiOI nanosheets: preparation, characterization and photocatalytic degradation activity, Appl. Surf. Sci., 423 (2017) 1188–1197.

[30] H.W. Huang, K. Liu, Y.L. Zhang, K. Chen, Y.H. Zhang, N. Tian, Tunable 3D hierarchical graphene-BiOI nanoarchitectures: their in situ preparation, and highly improved photocatalytic performance and photoelectrochemical properties under visible light irradiation, RSC Adv., 4 (2014) 49386–49394.

[31] D.M. Ma, J.B. Zhong, J.Z. Li, L. Wang, R.F. Peng, Enhanced photocatalytic activity of BiOCl by C70 modification and mechanism insight, Appl. Surf. Sci., 443 (2018) 497–505.

[32] Q. Yang, J. Huang, J.B. Zhong, J.F. Chen, J.Z. Li, S.Y. Sun, Charge separation behaviors of novel AgI/BiOI heterostructures with enhanced solar-photocatalytic performance, Curr. Appl. Phys., 17 (2017) 1202–1207.

[33] L. Lin, M.H. Huang, L.P. Long, Z. Sun, W. Zheng, D.H. Chen, Fabrication of a three-dimensional BiOBr/BiOI photocatalyst with enhanced visible light photocatalytic performance, Ceram. Int., 40 (2014) 11493–11501.

[34] M. Yang, Q. Yang, J.B. Zhong, S.T. Huang, J.Z. Li, J.B. Song, C. Burda, Enhanced photocatalytic performance of Ag_2O/BiOF composite photocatalysts originating from efficient interfacial charge separation, Appl. Surf. Sci., 416 (2017) 666–671.